AGU PUBLICATIONS

Geophysical Research Letters

RESEARCH LETTER
10.1002/2015GL066300

Special Section:
First Results from the MAVEN Mission to Mars

# A comet engulfs Mars: MAVEN observations of comet Siding Spring's influence on the Martian magnetosphere

**Jared R. Espley[1], Gina A. DiBraccio[1], John E. P. Connerney[1], David Brain[2], Jacob Gruesbeck[1,3], Yasir Soobiah[1,3], Jasper Halekas[4], Michael Combi[5], Janet Luhmann[6], Yingjuan Ma[7], Yingdong Jia[7], and Bruce Jakosky[2]**

[1]Laboratory for Planetary Magnetospheres, NASA Goddard Space Flight Center, Greenbelt, Maryland, USA, [2]Laboratory for Atmospheric and Space Physics, University of Colorado Boulder, Boulder, Colorado, USA, [3]Department of Astronomy, University of Maryland, College Park, Maryland, USA, [4]Department of Physics and Astronomy, University of Iowa, Iowa City, Iowa, USA, [5]Atmospheric, Oceanic and Space Sciences Department, University of Michigan, Ann Arbor, Michigan, USA, [6]Space Sciences Laboratory, University of California, Berkeley, California, USA, [7]Department of Earth, Planetary, and Space Sciences, University of California, Los Angeles, California, USA

**Key Points:**
- Comet Siding Spring's coma and plasma engulfed Mars on 19 October 2014
- The comet's plasma very likely severely distorted the Martian magnetosphere
- The comet might have driven atmospheric escape like a strong solar storm

**Correspondence to:**
J. R. Espley,
Jared.Espley@NASA.gov

**Citation:**
Espley, J. R., et al. (2015), A comet engulfs Mars: MAVEN observations of comet Siding Spring's influence on the Martian magnetosphere, *Geophys. Res. Lett.*, *42*, doi:10.1002/2015GL066300.

Received 25 SEP 2015
Accepted 10 OCT 2015

**Abstract** The nucleus of comet C/2013 A1 (Siding Spring) passed within 141,000 km of Mars on 19 October 2014. Thus, the cometary coma and the plasma it produces washed over Mars for several hours producing significant effects in the Martian magnetosphere and upper atmosphere. We present observations from Mars Atmosphere and Volatile EvolutioN's (MAVEN's) particles and field's instruments that show the Martian magnetosphere was severely distorted during the comet's passage. We note four specific major effects: (1) a variable induced magnetospheric boundary, (2) a strong rotation of the magnetic field as the comet approached, (3) severely distorted and disordered ionospheric magnetic fields during the comet's closest approach, and (4) unusually strong magnetosheath turbulence lasting hours after the comet left. We argue that the comet produced effects comparable to that of a large solar storm (in terms of incident energy) and that our results are therefore important for future studies of atmospheric escape, MAVEN's primary science objective.

## 1. Introduction

More than a million years ago, comet Siding Spring embarked on a journey from the Oort Cloud into the inner Solar System. A remarkable cosmic coincidence occurred on 19 October 2014 as its gaseous coma washed over Mars, temporarily displacing the solar wind. This event provided a unique opportunity to investigate the response of the induced Martian magnetosphere to extreme plasma conditions in the local space environment. Using data collected by instruments on board the MAVEN (Mars Atmosphere and Volatile EvolutioN) spacecraft, which arrived at Mars less than a month prior to this event, we are able to examine the interaction of comet Siding Spring with the Martian magnetosphere.

### 1.1. The Martian Magnetosphere

Since Mars currently lacks an intrinsic magnetic field, the charged plasma of the solar wind flows onto and around the upper Martian atmosphere. This interaction induces currents in the Martian ionosphere, which then act as the primary obstacle to the solar wind. This induced Martian magnetosphere shares many characteristics with classical magnetospheres but differs in others. A bow shock develops in the solar wind, followed by a region of shocked plasma called the magnetosheath. Below the magnetosheath, a separation occurs between the shocked solar wind and plasma of planetary origin. This boundary has had numerous names since its discovery, but in this letter, we use the term induced magnetospheric boundary (IMB) [*Lundin*, 2011]. It is also often called the magnetic pileup boundary [*Nagy et al.*, 2004]. Mars also has the complication of localized patches of comparatively strong magnetized crust [*Connerney et al.*, 2004] which produce mini-magnetospheres that can reach up to 1000 km in altitude. See the reviews by *Nagy et al.* [2004], *Dubinin et al.* [2006], and *Brain et al.* [2015] for more details and the lower right of Figure 1 for a rough schematic for scale.

### 1.2. Comets and Their Plasma

Cometary nuclei are commonly described as chunks of dirty ice roughly 10 km in size. Cometary ice is sublimated by the Sun and escapes from the nucleus with velocities of order 1 km/s, forming a gaseous coma around the

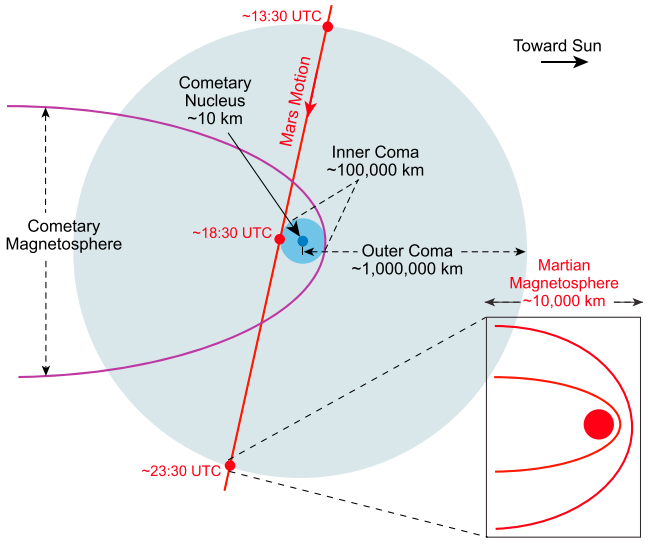


**Figure 1.** A schematic diagram (approximately to scale) of the interaction of comet Siding Spring with the Martian magnetosphere.

nucleus [*Combi et al.*, 2004]. Far from the nucleus, the gas molecules no longer collide and they follow ballistic trajectories spreading out in an approximate sphere. Solar UV is the dominant mechanism for ionization, and the reaction time for this interaction is roughly $10^6$ s, so a typical cometary gas molecule travels $10^6$ km before being ionized [*Cravens and Gombosi*, 2004]. At this point, the cometary ion is subject to electromagnetic forces, and it is picked up by the solar wind and swept away from the Sun. The addition of cometary plasma "steals" momentum from the solar wind, and it slows in the vicinity of the comet, forming a bow shock and a cometary magnetosphere [*Luhmann et al.*, 1988; *Ip*, 2004; *Coates and Jones*, 2009].

In summary (Figure 1), surrounding the cometary nucleus there exists an extended gas cloud of which the inner part is dense enough to be seen remotely (e.g., with telescopes) [*A'Hearn et al.*, 1995]. This "inner coma" typically has a radius of order 100,000 km. An outer part of the coma ("outer coma") extends until all significant quantities of gas have been ionized and swept away; it has a radius of order of $10^6$ km. Throughout the coma, the plasma being created produces the ion tail and more generally the cometary magnetosphere. For a moderately inactive comet, the magnetospheric bow shock is about 20,000 km from the nucleus at the subsolar point [*Coates et al.*, 1997].

### 1.3. Comet Siding Spring

Comet C/2013 A1 (Siding Spring), referred to as comet Siding Spring hereafter, was discovered on 3 January 2013 by Robert McNaught at the Siding Spring Observatory in Australia [*McNaught et al.*, 2013]. It is a dynamically new comet [cf. *Farnocchia et al.*, 2014, Table 1], meaning that it is on its first (and likely only) passage through the inner Solar System after leaving the Oort Cloud more than $10^6$ years ago. Like all comets, comet Siding Spring's gas production rate increased as it approached the Sun. However, in the weeks before its closest approach to Mars, this rate level lessened slightly [*Lisse and CIOC Team*, 2015], and it was producing approximately $1 \times 10^{28}$ water molecules per second during the time of closest approach [*Schleicher et al.*, 2014; *Bodewits et al.*, 2015]. This made it a relatively inactive comet, comparable to comet Grigg-Skjellerup [*Johnstone et al.*, 1993; *Coates et al.*, 2015]. It nonetheless had appreciable effects on the Martian magnetosphere as we discuss below.

## 2. The MAVEN Mission

The MAVEN mission's primary science objective is to investigate the possibility that the solar wind has gradually blown away the bulk of the Martian atmosphere over the past few billion years [*Jakosky and Phillips*, 2001]. In order to do so, MAVEN is designed to robustly characterize the current interaction between the Martian atmosphere and the solar wind [*Jakosky et al.*, 2015a]. It thus carries an instrument complement to understand the solar inputs into the system and to identify and characterize all planetary constituents above the well-mixed lower atmosphere. These characteristics also make it a remarkably well-suited mission to study the interaction of a comet with the Martian magnetosphere.

MAVEN arrived at Mars on 22 September 2014. All science instruments were turned on and fully deployed by 10 October 2014. Nine days later, comet Siding Spring made its closest approach to Mars on 19 October 2014 (day of year 292). To prepare for the comet encounter, precautions were exercised in order to protect the spacecraft from macroscopic dust (millimeter sized or larger) in the cometary tail, which would be moving

at an approximate relative velocity of 56 km/s. Early estimates of the number and mass densities of the dust [*Vaubaillon et al*., 2014; *Moorhead et al*., 2014; *Ye and Hui*, 2014] were handicapped by limited observations but were alarming since such "hypervelocity" impacts can easily damage spacecraft as well as produce measurable local plasmas [e.g., *Neubauer et al*., 1990; *Goldstein et al*., 1991]. Later estimates, based on more comprehensive observations, suggested that the danger was statistically similar to the likelihood of a micrometeorite hit over the expected mission lifetime [*Kelley et al*., 2014; *Tricarico et al*., 2014]. In anticipation of this dust the precautions included timing the orbits such that the spacecraft was protected behind the planet when the dust tail arrived along with turning the solar arrays edge on with respect to the dust, to minimize the exposed surface area. Direct impacts on spacecraft components were a major concern, but the MAVEN project also decided to turn off any instruments with high voltages or optics in order to avoid danger from debris associated with impacts anywhere on the spacecraft. This left just the magnetometer (MAG), the Langmuir Probe and Waves (LPW) instrument, and the Solar Energetic Particles (SEP) instrument on for the orbit during the comet's closest approach (approximately 16:30–22:00 UTC). LPW was in a mode primarily designed to characterize the dust, and the comet was not expected to directly produce effects detectable by SEP. For this reason, we focus in this paper on the MAG data for observing effects on the Martian magnetosphere during the comet's closest approach. We also use the Solar Wind Ion Analyzer (SWIA) instrument to provide context on the character of the solar wind before and after the closest approach.

The magnetometer investigation [*Connerney et al*., 2015a] consists of two fluxgate magnetometers (which provide hardware redundancy and increased spacecraft magnetic control diagnostics). The MAG data used here were acquired at 32 vector samples per second with a measured maximum of ±512 nT in the primary range (±2048 nT in the secondary range) giving it an approximate digital resolution of 8 pT. The data have been carefully calibrated and corrected for minor spacecraft-generated spacecraft fields [*Connerney et al*., 2015b].

The SWIA instrument [*Halekas et al*., 2013] is an electrostatic analyzer designed specifically to study ions with energies from 5 eV to 26 keV. The data set used here is the omnidirectional differential energy flux (eV/(eV $cm^2$ s sr)) which has a maximum time cadence of every 4 s in 48 energy bins across the full energy range. The instrument measures the energy of the ions but does not distinguish between mass. Normally, this function is provided by other instruments on board MAVEN but as discussed these instruments were off during the comet's passage so the nature of the ions measured must be inferred by the context of the observations (i.e., if upstream of the bow shock then the ions are likely solar wind protons).

MAVEN's orbit carries it through all the regions of the magnetosphere with an apoapsis of about 6000 km, a periapsis of about 150 km, and an orbital period of about 4.5 h. A coordinate system often used to understand the magnetosphere is the Mars Solar Orbital (MSO) coordinate system also known as the Sun-State coordinate system. In this system, $x$ points toward the Sun, $y$ in the direction opposite of Mars' orbital motion, and $z$ completes the orthogonal set and is approximately north.

## 3. Observations

For 2 weeks before 18 October, conditions in the Martian magnetosphere were approximately nominal (the magnetosheath $|B|$ was about 10 nT, the draped dayside ionospheric $|B|$ was about 40 nT, and the magnetosheath ion density was about 10 particles/$cm^3$). Then on 18 October at approximately 01:00 UTC, an interplanetary coronal mass ejection (ICME) hit Mars. The SWIA data at that time show elevated densities of approximately 20 particles/$cm^3$. The peak energy ions (~1 keV) increased in the differential flux from ~$10^7$ to ~$10^8$, and the energy range of that peak broadened to encompass a range of about 500 eV–5 keV. The MAG data show a draped dayside $|B|$ of approximately 140 nT, which was unrelated to crustal fields (based on a comparison with a spherical harmonic model of the crustal field [*Morschhauser et al*., 2014]) and an increase in the magnetosheath turbulence.

These elevated signatures due to the ICME gradually diminished over the next six MAVEN orbits. By the second periapsis of 19 October around 06:00 UTC conditions had returned to that of the nominal magnetospheric configuration. As seen in Figure 2, the energy spectra were comparatively reduced in peak flux, the draped magnetic field declined in magnitude to about 40 nT, and the magnetosheath turbulence relaxed to nominal levels.

At about 13:30 UTC on 19 October, Mars entered the outer coma of comet Siding Spring, then at 18:28 UTC Mars passed within about 141,000 km of the nucleus, and finally at 23:30 UTC Mars exited the other side of

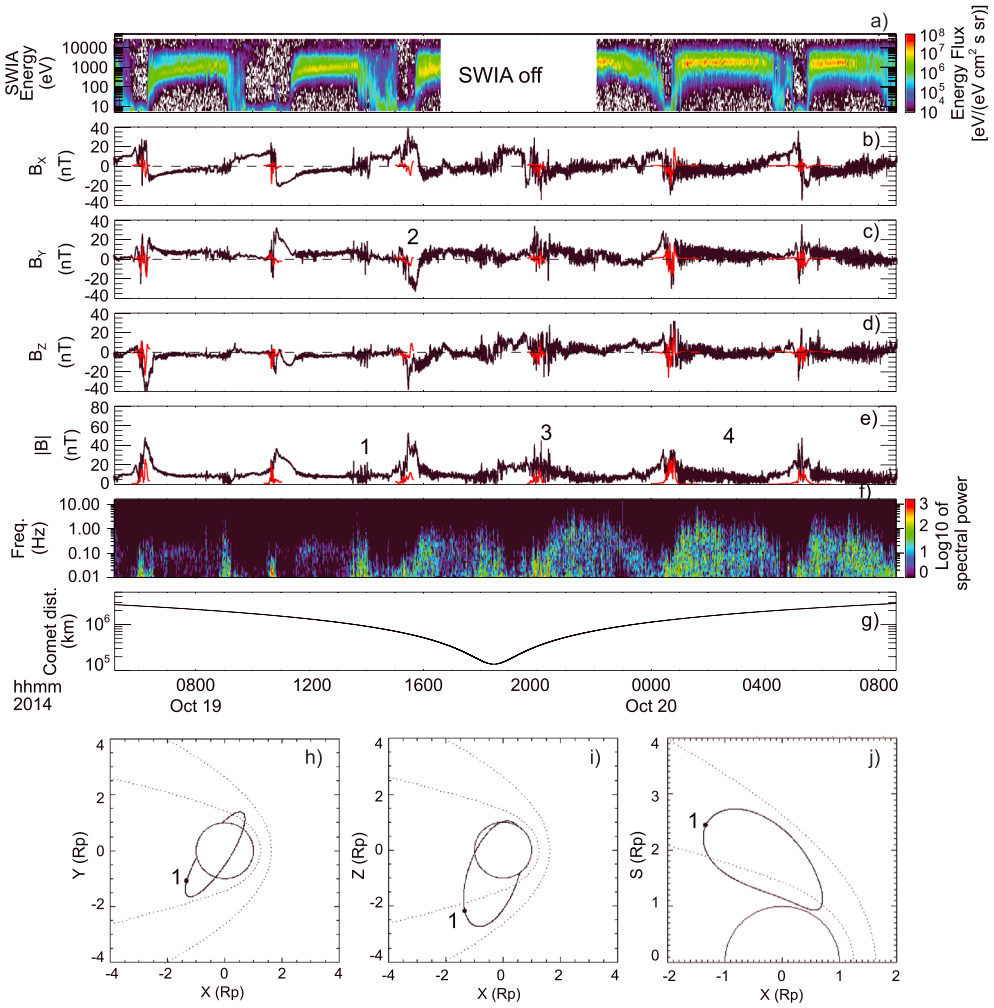


**Figure 2.** A set of time series data for the 26 h around the comet's closest approach. (a) The SWIA differential energy flux spectra. (b–e) The magnetic field components and magnitude. The red lines show the modeled crustal field contributions [*Morschhauser et al.*, 2014] at those locations. (f) A wavelet spectrum [*Torrence and Compo*, 1998] of $|B|$. (g) The distance between the comet nucleus and Mars. (h–j) The location of MAVEN in MSO coordinates with units of Mars radii during event 1 (section 3.1). The dashed lines show the nominal bow shock and IMB and the solid line MAVEN's orbit which, since MAVEN's orbit changes slowly, is accurate for all orbits under consideration here. Figure 2j shows this location in a cylindrical projection of MSO coordinates, where $S = \sqrt{Y^2 + Z^2}$. Four notable events are marked with numbers and discussed in the text.

the outer coma. This timing is shown in Figure 1. From the perspective of the comet, Mars passed downstream of the nucleus just on the outer edge of the inner coma. Also, note the relative size of the Martian magnetosphere compared to the cometary comas and magnetosphere. From the perspective of Mars (not shown), the comet approached from the Sun's direction (MSO $x$), from below Mars' orbit plane (MSO $-z$), and from the direction of Mars' orbital motion (MSO $-y$). Although still slightly accelerating (since it reached its perihelion 5 days later), the comet's approach velocity was approximately 56 km/s during the whole encounter with Mars.

Thus, it seems likely that the unusual signatures seen during the comet's passage (described below in sections 3.1) can be attributed to the comet's influence. Nonetheless, it is difficult to completely rule out other causes, such as lingering effects from the ICME or an ill-timed arrival of general solar wind disturbances. However, we find the timings of our four major signatures (coincident with the arrival of different parts of the comet's plasma) to be compelling. Our estimates of the cometary plasma energy influx (see section 4) and the preliminary MHD models of the interaction [*Ma et al.*, 2014] add further weight to

our interpretation. Our interpretation that Martian magnetosphere had returned to nominal conditions approximately 30 h after the ICME's arrival (i.e., by 06:00 UTC on 19 October) is roughly consistent with the limited observations of the durations of ICME effects at Mars [*Crider et al*., 2005; *Morgan et al*., 2014]. As MAVEN observes more space weather events (e.g., more ICMEs), we will be able to more fully disentangle the effects from those events from those caused by the heavy cometary plasma.

### 3.1. Perturbations Near the Induced Magnetospheric Boundary

At about 13:30 UTC (marked #1 in Figure 2), MAG and SWIA observed a series of unusual perturbations. Figures 2h–2j show that MAVEN was in a location that is normally the southern nightside magnetosheath. The background field was about 9 nT, but several of the perturbations had magnitudes of up to 25 nT. The wavelet spectra show that the predominant frequency was at or below 0.01 Hz although there was activity at other, higher frequencies.

To further confirm the unusual nature of these perturbations, we examined 80 orbits from 10 to 25 October (i.e., approximately 1 week before and after the comet's closest approach which means that all of the orbits had very similar geometries in MSO coordinates). We looked at data intervals for each of the 80 orbits that corresponded to the location where we saw the unusual perturbations. This meant using intervals that were at altitudes above 3000 km and with solar zenith angles (SZAs) between 100° and 125°. We found the RMS of the field variability at timescales of 5 min (roughly the spacing interval between the perturbations). For all 80 intervals, the mean RMS is 1.7 with a standard deviation of 0.9 nT. For the interval from 13:30 to 14:15 UTC, the RMS is 4.9 with a standard deviation of 1.3 nT. The results were qualitatively the same for any RMS timescale between 1 and 10 min. Visual inspection of the intervals and their RMS confirmed that the only other interval with 5 min variability comparable to the interval under consideration was the one just after the arrival of the ICME on 18 October.

Suggestively, these perturbations occurred just as Mars entered the predicted outer coma of the comet. The wave activity at about 0.1 Hz prior to the perturbations (from ~12:00 to 13:00 UTC) is typical for the magnetosheath [*Espley et al*., 2004]. These "normal" magnetosheath waves are associated with proton cyclotron waves in resonance with a $|B|$ of approximately 10 nT, and their cessation is a characteristic signature of the passage into the induced magnetospheric boundary [*Vignes et al*., 2000]. Similarly, the SWIA data show the semi-monoenergetic spectra of about 1 keV ions which then disappear at the location of the perturbations. So the unusual perturbations occur near the presumptive location of the induced magnetospheric boundary. We therefore tentatively interpret these perturbations as evidence of a time variable induced magnetospheric boundary due to the outer coma's plasma interacting with Mars. One specific possibility for the physical mechanism at work is the Kelvin-Helmholtz instability which develops when there is differential velocity across two dissimilar fluids. Such instabilities have been seen before in the Martian ionosphere [*Penz et al*., 2004; *Gurnett et al*., 2010], but detailed analysis of these perturbations will await future work.

### 3.2. Strong and Prolonged Realignment of the Draped Magnetic Field

At approximately 15:30 UTC, the draped magnetic field experienced a highly unusual reorientation, which shows most prominently as a strong and prolonged reversal into the $-y$ MSO direction (marked #2 in Figure 2). During the same 80 orbits examined in section 3.1, no such reversal with the same magnitude or duration was observed.

Figures 3b, 3e, and 3h show the orientation of the magnetic field from the data around periapsis of this orbit (called comet orbit #1 hereafter), while Figures 3a, 3d, and 3g show the orientation for the prior periapsis (called the pre-comet orbit hereafter). The pre-comet orbit clearly shows an orderly field with two lobes which is expected since the interplanetary magnetic field is draped around the obstacle of the ionosphere. Comet orbit #1 is still fairly ordered, but the fields are oriented in roughly the same directions throughout the periapsis and have strongly reversed directions in the $+Y$ side of the orbit—the side opposite of the incoming cometary magnetosphere. Given the timing of the orbit (near when the relatively ordered portions of the outer cometary magnetosphere would be moving over the planet), we interpret this reorientation as being driven by the arrival of the magnetic field associated with the comet and its draping over the planet. Detailed modeling, such as the MHD model given by *Ma et al*. [2015], should help elucidate the situation.

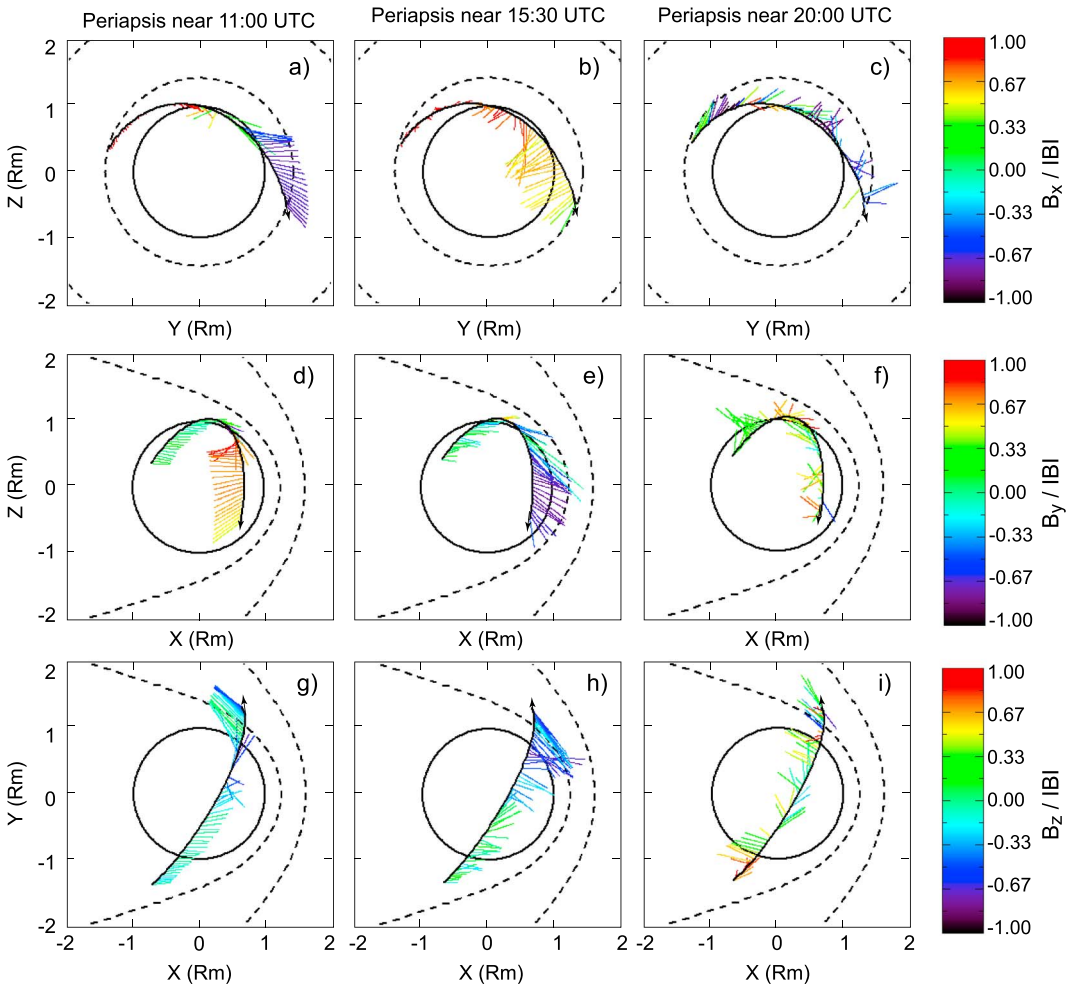


**Figure 3.** The direction and strength of the magnetic fields in MSO coordinates for three orbits. For each orbit all data from below 2000 km are shown. (a, d, and g) The orbit just before the comet arrived. (b, e, and h) The orbit as the comet was arriving. (c, f, and i) The orbit during the comet's closest approach. In all panels, the length of the colored "whiskers" is normalized to the maximum value for the interval and 1 min of data are averaged together to show one whisker. The color indicates the normalized strength of the component into or out of the plane shown. The solid dark line with the arrow indicates the direction of the MAVEN orbit. The dashed lines show the nominal bow shock and induced magnetospheric boundaries [*Trotignon et al.*, 2006].

### 3.3. A Damped and Highly Disturbed Field During Closest Approach

During the orbit of the comet's closest approach, the magnetic field was clearly abnormal (marked #3 in Figure 2). From a broad perspective, two specific features stand out. The dayside peak field is lower than normal, and conversely, the low-altitude nightside field is higher than normal. This gives the periapsis a low, broad profile instead of the usual asymmetric, sharply peaked profile.

To further quantify the uniqueness of this periapsis, we examined our set of 80 adjacent orbits. Excluding the orbits from 18 October (when the ICME hit) and 19 October (the day of the comet), we found that for the remaining 70 orbits, at altitudes less than 1000 km and SZA less than 75° (e.g., the dayside) that the mean $|B|$ was 22 nT with a standard deviation of 10 nT. For the periapsis of the comet's closest approach, the same criteria gave a $|B|$ of 17 nT with a standard deviation of 4 nT. For the same altitude range but for SZAs greater than 75° (e.g., on the nightside), we found that the adjacent orbits had a mean $|B|$ of 15 nT with a standard deviation of 9 nT, whereas the field during the comet's approach was $|B|$ of 17 nT with a standard deviation of 4 nT. Thus, the quantitative comparison confirms what is discernible by eye—the dayside field during the comet's closest approach is reduced (i.e., by about 25% from the nominal), whereas

the nightside field is enhanced. A plausible explanation for the dayside result is that the enhanced plasma pressure from the heavier cometary plasma damped the normal dayside fields.

Numerous unusual, small-scale structures are present within this broader picture. Several large $|B|$ excursions (some as large as 45 nT) punctuate the otherwise diminished periapsis fields. There are associated rotations in the vector magnetic field, and these excursions are likely due to ionospheric flux ropes created by the turbulent conditions [*Vignes et al*., 2004]. In other intervals, there are unusual segments with durations of about 30 s in which $|B|$ is relatively low (~5 nT) but unusually steady. These segments are surrounded by fields of higher magnitude giving them the profile of a canyon.

The field orientations shown in Figures 3c, 3f, and 3i reinforce this picture of an unusual and turbulent interaction. While the periapsis as the comet was approaching (comet orbit #1) shows a strong rotation of the field compared to the periapsis that occurred before the comet, it was still relatively ordered. The periapsis during the comet's closest approach (comet orbit #2), in contrast, shows little organization by geometry but instead appears as a series of scattered fields.

### 3.4. Prolonged Turbulence After the Comet's Departure

The first three outbound magnetosheath crossings after the comet's closest approach were filled with extraordinary turbulence (the second crossing is marked with a #4 in Figure 2). While the Martian magnetosheath is normally filled with significant low-frequency magnetic oscillations [*Espley et al*., 2004; *Ruhunusiri et al*., 2015], these fluctuations are abnormally large ($\delta B$ about 5 nT with a background $|B|$ of about 5 nT) and unusually have significant spectral power at frequencies above 0.1 Hz (Figure 2f). For the magnetosheath at the SZAs where these observations are made (60° to 130°) the typical $\delta B$ is 1–2 nT.

Nonetheless, initial analysis indicates that the fluctuations are a mixture of wave modes as is typical for the magnetosheath but are primarily associated with proton cyclotron waves. While it is certainly striking how clearly they start as the comet makes its closest approach (e.g., Figure 2f), it is surprising that they would persist long after the comet has left the system (i.e., after ~06:00 UTC 20 October). The typical timescales for the transfer of energy through the Martian magnetosphere might be expected to scale with the Alfvén speed and thus be minutes or at most hours. Nonetheless, it is plausible that they represent some sort of relaxation mechanism for dissipating the comet's energy long after its direct influence has been removed.

## 4. Discussion and Summary

In order to interpret the observations presented above, we make some order of magnitude estimates of how the cometary plasma compares with the solar wind. First, if we assume that the cometary gas production rate is $1 \times 10^{28}$ $H_2O$ molecules/s and that the molecules' ejection speed is 1 km/s and isotropic then we can calculate that at $10^6$ km away from the nucleus the density of cometary gas is approximately equal to the solar wind density at Mars (1 particle/cm$^3$). Some fraction of this gas will actually be lost to ionization before that, but some fraction of the gas upstream of that point will have been ionized and swept downstream to that point. The details of this would require more sophisticated modeling [*Daly*, 1989, 1991], but it is reasonable to assume that the ion density would be at least a few percent of the gas density at a distance of $10^6$ km since the ionization length scale is $10^6$ km. Although photochemistry will change the composition of the released water ions, there will be ions with a mass of 18 amu moving downstream with the approximate velocity of the solar wind since they will have been electromagnetically picked up. Therefore, at $10^6$ km from the comet, it is reasonable to assume that the kinetic energy per volume of the comet's plasma is comparable to that of the solar wind. As shown in Figure 1, this is where we have defined the outer coma of the comet and Mars passed into this region at approximately 13:30 UTC.

Similarly, again using simple isotropic expansion, at the distance of closest approach (141,000 km) the gas density should be of order 100 particles/cm$^3$ (the inner coma shown in Figure 1). The percentage actually locally ionized at this point depends on the details of the photochemistry. But given the interaction geometry, the full upstream hemisphere of ionized gas should also be sweeping over Mars. Therefore, combining an ion density that is a few percent of the gas density with the fact the comet ions are generally 18 times more massive than the solar wind ions gives an expected energy density for the cometary plasma of order 100 times the normal solar wind energy density. This is comparable to a very significant solar

weather event. For example, the 8 March 2015 interplanetary coronal mass ejection (ICME) that hit Mars [*Jakosky et al*., 2015b] had an energy density of approximately 40 times that of the normal solar wind. Thus, it seems reasonable to conclude that the observational features shown in section 3 could have been caused by the comet.

Several avenues for future work present themselves. First, clearly detailed analysis, beyond the scope of this initial survey, should be done for all of the unusual features observed. In this respect, utilizing some of the other data sets not included here such as the Solar Wind Electron Analyzer and the Suprathermal and Thermal Ion Composition instrument would be helpful even though they did not collect data during the entire interval of interest. Utilization of global models such as the MHD model of *Ma et al*. [2015] should allow greater physical insight and testing of hypotheses. Perhaps most importantly, we will be able to better contextualize these observations as we observe more episodes of significant space weather events at Mars. MAVEN's primary science goal of understanding atmospheric escape at Mars depends crucially on understanding how the erosion from large but infrequent events compares to that of the small but steady erosion of the nominal solar wind. It is truly good fortune that a highly unusual and potentially highly eroding event occurred at Mars weeks after MAVEN arrived. We look forward to gaining further insight into how comet Siding Spring distorted the Martian magnetosphere and estimating how much atmospheric loss it caused.

**Acknowledgments**
The MAVEN project is supported by NASA through the Mars Exploration Program. DiBraccio was supported by a NASA Postdoctoral Program appointment at the NASA Goddard Space Flight Center, administered by Oak Ridge Associated Universities through a contract with NASA. MAVEN data are publicly available through the Planetary Data System. The wavelet analysis software used in this work was based on software provided by C. Torrence and G. Compo and is available at http://paos.colorado.edu/research/wavelets/. The MAVEN spacecraft staff at Lockheed Martin worked diligently under stressful circumstances to make sure the data during the comet's closest approach were collected for the science team. Their efforts and sacrifices are sincerely appreciated. The authors sincerely thank the careful, thoughtful, and polite reviewers whose suggestions made the paper better.

## References

A'Hearn, M. F., R. C. Millis, D. O. Schleicher, D. J. Osip, and P. V. Birch (1995), The ensemble properties of comets: Results from narrowband photometry of 85 comets, 1976–1992, *Icarus*, *118*, 223–270, doi:10.1006/icar.1995.1190.

Bodewits, D., M. S. P. Kelley, J. Li, T. L. Farnham, and M. F. A'Hearn (2015), The pre-perihelion activity of dynamically new comet C/2013 A1 (Siding Spring) and its close encounter with Mars, *Astrophys. J. Lett.*, *802*, L6, doi:10.1088/2041-8205/802/1/L6.

Brain, D. A., S. Barabash, S. Bougher, F. Duru, B. Jakosky, and R. Modolo (2015), Solar wind interaction and atmospheric escape, in *The Mars Atmosphere*, edited by B. Haberle et al., Cambridge Univ. Press, Cambridge, in press.

Coates, A. J., and G. H. Jones (2009), Plasma environment of Jupiter family comets, *Planet. Space Sci.*, *57*, 1175–1191, doi:10.1016/j.pss.2009.04.009.

Coates, A. J., C. Mazelle, and F. M. Neubauer (1997), Bow shock analysis at comets Halley and Grigg-Skjellerup, *J. Geophys. Res.*, *101*, 7105–7114, doi:10.1029/96JA04002.

Coates, A. J., A. Wellbrock, R. A. Frahm, J. D. Winningham, A. Federov, S. Barabash, and R. Lundin (2015), Distant ionospheric photoelectron energy peak observations at Venus, *Planet. Space Sci.*, *113*, 378–384, doi:10.1016/j.pss.2015.02.003.

Combi, M. R., W. M. Harris, and W. H. Smyth (2004), Gas dynamics and kinetics in the cometary coma: Theory and observations, in *Comets II*, edited by M. C. Festou, H. U. Keller, and H. A. Weaver, pp. 523–552, Univ. of Arizona Press, Tucson.

Connerney, J. E. P., M. H. Acuña, N. F. Ness, T. Spohn, and G. Schubert (2004), Mars crustal magnetism, *Space Sci. Rev.*, *111*(1–2), 1–32.

Connerney, J. E. P., J. Espley, P. Lawton, S. Murphy, J. Odom, R. Oliversen, and D. Sheppard (2015a), The MAVEN magnetic field investigation, *Space Sci. Rev.*, doi:10.1007/s11214-015-0169-4.

Connerney, J. E. P., J. R. Espley, G. A. DiBraccio, J. R. Gruesbeck, R. J. Oliversen, D. L. Mitchell, J. Halekas, C. Mazelle, D. Brain, and B. M. Jakosky (2015b), First results of the MAVEN magnetic field investigation, *Geophys. Res. Lett.*, *42*, doi:10.1002/2015GL065366.

Cravens, T. E., and T. I. Gombosi (2004), Cometary magnetospheres: A tutorial, *Adv. Space Res.*, *33*, 1968–1976, doi:10.1016/j.asr.2003.07.053.

Crider, D. H., J. Espley, D. A. Brain, D. L. Mitchell, J. E. P. Connerney, and M. H. Acuña (2005), Mars Global Surveyor observations of the Halloween 2003 solar superstorm's encounter with Mars, *J. Geophys. Res.*, *110*, A09S21, doi:10.1029/2004JA010881.

Daly, P. W. (1989), The use of Kepler trajectories to calculate ion fluxes at multi-gigameter distances from Comet Halley, *Astron. Astrophys.*, *226*, 318–334.

Daly, P. W. (1991), Model calculations of oxygen ion fluxes from the dissociation of $H_2O$, CO, and $CO_2$ at gigameter distances from Comet Halley, in *Cometary Plasma Processes*, edited by A. Johnstone, AGU, Washington, D. C., doi:10.1029/GM061p0341.

Dubinin, E., M. Fränz, J. Woch, E. Roussos, S. Barabash, R. Lundin, J. D. Winningham, R. A. Frahm, and M. Acuña (2006), Plasma morphology at Mars. Aspera-3 observations, *Space Sci. Rev.*, *126*, 209–238, doi:10.1007/s11214-006-9039-4.

Espley, J. R., P. A. Cloutier, D. A. Brain, D. H. Crider, and M. H. Acuña (2004), Observations of low-frequency magnetic oscillations in the Martian magnetosheath, magnetic pileup region, and tail, *J. Geophys. Res.*, *109*, A07213, doi:10.1029/2003JA010193.

Farnocchia, D., S. Chesley, P. W. Chodas, P. Tricarico, M. S. P. Kelley, and T. L. Farnham (2014), Trajectory analysis for the nucleus and dust of Comet C/2013 A1 (Siding Spring), *Astrophys. J.*, *790*, 114, doi:10.1088/0004-637X/790/2/114.

Goldstein, R., B. E. Goldstein, H. Balsiger, A. J. Coates, W. Curdt, H. U. Keller, F. M. Neubauer, C. Perry, and J. Zarnecki (1991), The composition and plasma signature of a large dust impact on the Giotto spacecraft, *J. Geophys. Res.*, *96*(A8), 13,739–13,747, doi:10.1029/91JA01013.

Gurnett, D. A., D. D. Morgan, F. Duru, F. Akalin, J. D. Winningham, R. A. Frahm, E. Dubinin, and S. Barabash (2010), Large density fluctuations in the Martian ionosphere as observed by the Mars Express radar sounder, *Icarus*, *206*(1), 83–94, doi:10.1016/j.icarus.2009.02.019.

Halekas, J. S., E. R. Taylor, G. Dalton, G. Johnson, D. W. Curtis, J. P. McFadden, D. L. Mitchell, R. P. Lin, and B. M. Jakosky (2013), The solar wind ion analyzer for MAVEN, *Space Sci. Rev.*, doi:10.1007/s11214-013-0029-z.

Ip, W. H. (2004), Global solar wind interaction and ionospheric dynamics, in *Comets II*, edited by M. C. Festou, H. U. Keller, and H. A. Weaver, pp. 605–629, Univ. of Arizona Press, Tucson.

Jakosky, B. M., and R. J. Phillips (2001), Mars' volatile and climate history, *Nature*, *412*, 237–244, doi:10.1038/35084184.

Jakosky, B. M., et al. (2015a), The Mars Atmosphere and Volatile EvolutioN (MAVEN) mission, *Space Sci. Rev.*, doi:10.1007/s11214-015-0139-x.

Jakosky, B. M., et al. (2015b), MAVEN observations of the response of Mars to an interplanetary coronal mass ejection, *Science*, doi:10.1126/science.aad0210.

Johnstone, A. D., A. J. Coates, D. E. Huddleston, K. Jockers, B. Wilken, H. Borg, C. Gurgiolo, J. D. Winningham, and E. Amata (1993), Observations of the solar wind and cometary ions during the encounter between Giotto and Comet Grigg-Skjellerup, *Astron. Astrophys.*, *273*, L1–L4.

Kelley, M. S. P., T. L. Farnham, D. Bodewits, T. Pasquale, and D. Farnocchia (2014), A study of dust and gas at Mars from Comet C/2013 A1 (Siding Spring), *Astrophys. J. Lett.*, *792*, L16, doi:10.1088/2041-8205/792/1/L16.

Lisse, C. M., and the CIOC Team (2015), Results from the CIOC Comet Siding Spring at Mars observing campaign, presented at the 46th Lunar and Planetary Science Conference, The Woodlands, Tex.

Luhmann, J. G., J. A. Fedder, and D. Winske (1988), A test particle model of pickup ions at comet Halley, *J. Geophys. Res.*, *93*(A7), 7532–7537, doi:10.1029/JA093iA07p07532.

Lundin, R. (2011), Ion acceleration and outflow from Mars and Venus: An overview, *Space Sci. Rev.*, *162*, 309–334, doi:10.1007/s11214-011-9811-y.

Ma, Y., Y. D. Jia, C. T. Russell, A. F. Nagy, G. Toth, M. R. Combi, R. V. Yelle, C. Dong, and S. W. Bougher (2014), The Mars magnetosphere in the tail of Comet C/2013 A1(Siding Spring), presented at the Fall AGU Meeting, San Francisco, Calif.

Ma, Y. J., C. T. Russell, A. F. Nagy, G. Toth, J. S. Halekas, J. E. P. Connerney, J. R. Espley, and P. R. Mahaffy (2015), MHD model results of solar wind plasma interaction with Mars and comparison with MAVEN observations, presented at the 46th Lunar and Planetary Science Conference, The Woodlands, Tex.

McNaught, R. H., H. Sato, and G. V. Williams (2013), Comet C/2013 A1 (Siding Spring), Cent. Bureau Electr. Telegrams, 3368, 1.

Moorhead, A. V., P. A. Wiegert, and W. J. Cooke (2014), The meteoroid fluence at Mars due to comet C/2013 A1 (Siding Spring), *Icarus*, *231*, 13–21, doi:10.1016/j.icarus.2013.11.028.

Morgan, D. D., et al. (2014), Effects of a strong ICME on the Martian ionosphere as detected by Mars Express and Mars Odyssey, *J. Geophys. Res. Space Physics*, *119*, 5891–5908, doi:10.1002/2013JA019522.

Morschhauser, A., V. Lesur, and M. Grott (2014), A spherical harmonic model of the lithospheric magnetic field of Mars, *J. Geophys. Res. Planets*, *119*, 1162–1188, doi:10.1002/2013JE004555.

Nagy, A., et al. (2004), The plasma environment of Mars, *Space Sci. Rev.*, *111*, 33–114, doi:10.1023/B:SPAC.0000032718.47512.92.

Neubauer, F. M., K.-H. Glassmeier, A. J. Coates, R. Goldstein, M. H. Acuña, and G. Musmann (1990), Hypervelocity dust particle impacts observed by the Giotto magnetometer and plasma experiments, *Geophys. Res. Lett.*, *17*(11), 1809—1812, doi:10.1029/GL017i011p01809.

Penz, T., N. V. Erkaev, H. K. Biernat, and H. Lammer (2004), Ion loss on Mars caused by the Kelvin-Helmholtz instability, *Planet. Space Sci.*, *52*, 1157–1167, doi:10.1016/j.pss.2004.06.001.

Ruhunusiri, S., J. S. Halekas, J. E. P. Connerney, J. R. Espley, J. P. McFadden, D. E. Larson, D. L. Mitchell, C. Mazelle, and B. M. Jakosky (2015), Low-frequency waves in the Martian magnetosphere and their response to upstream solar wind driving conditions, *Geophys. Res. Lett.*, *42*, doi:10.1002/2015GL064968.

Schleicher, D., M. Knight, and B. Skiff (2014), Comet C/2013 A1 (Siding Spring), Cent. Bureau Electr. Telegrams, 4004, 1.

Torrence, C., and G. P. Compo (1998), A practical guide to wavelet analysis, *Bull. Am. Meteorol. Soc.*, *79*, 61–78, doi:10.1175/1520-0477(1998)079<0061:APGTWA>2.0.CO;2.

Tricarico, P., N. H. Samarasinha, M. V. Sykes, J.-Y. Li, T. L. Farnham, M. S. P. Kelley, D. Farnocchia, R. Stevenson, J. M. Bauer, and R. E. Lock (2014), Delivery of dust grains from comet C/2013 A1 (Siding Spring) to Mars, *Astrophys. J. Lett.*, *787*, L35, doi:10.1088/2041-8205/787/2/L35.

Trotignon, J. G., C. Mazelle, C. Bertucci, and M. H. Acuña (2006), Martian shock and magnetic pile-up boundary positions and shapes determined from the Phobos 2 and Mars Global Surveyor data sets, *Planet. Space Sci.*, *54*, 357–369, doi:10.1016/J.Pss.2006.01.003.

Vaubaillon, J., L. Maquet, and R. Soja (2014), Meteor hurricane at Mars on 2014 October 19 from comet C/2013 A1, *MNRAS*, *439*(4), 3294–3299, doi:10.1093/mnras/stu160.

Vignes, D., C. Mazelle, H. Rme, M. H. Acuña, J. E. P. Connerney, R. P. Lin, D. L. Mitchell, P. Cloutier, D. H. Crider, and N. F. Ness (2000), The solar wind interaction with Mars: Locations and shapes of the bow shock and the magnetic pile-up boundary from the observations of the MAG/ER experiment onboard Mars Global Surveyor, *Geophys. Res. Lett.*, *27*, 49–52, doi:10.1029/1999GL010703.

Vignes, D., M. H. Acuña, J. E. P. Connerney, D. H. Crider, H. Rème, and C. Mazelle (2004), Magnetic flux ropes in the Martian atmosphere: Global characteristics, *Space Sci. Rev.*, *111*, 223–231, doi:10.1023/B:SPAC.0000032716.21619.f2.

Ye, Q.-Z., and M.-T. Hui (2014), An early look of comet C/2013 A1 (Siding Spring): Breathtaker or nightmare?, *Astrophys. J.*, *787*, 115, doi:10.1088/0004-637X/787/2/115.